

Effect of Filler Size on Porosity of Porous Parts Obtained Via PBF-LB/P and Filler Dissolution

Koichi Fujii, Takashi Kigure, Ryuichi Kobayashi, Yuki Yamauchi

Tokyo Metropolitan Industrial Technology Research Institute, 2-4-10 Aomi Koto-ku, Tokyo,
Japan

Abstract

This study investigates the fabrication of porous parts using polyamide 12 (PA12) in a polymer-based powder bed fusion process with a laser beam (PBF-LB/P), where a powder containing a soluble filler is laser-sintered and subsequently subjected to filler dissolution. The porosity of the parts after dissolution could be controlled by varying the filler content. However, the porosity and filler content are typically not equivalent because pores may also result from insufficient powder flow, incomplete fusion, or partial dissolution during laser sintering. This study discusses the effect of filler size on powder properties and part porosity before dissolution. NaCl was mixed with polyamide 12 powder as a soluble filler for different particle sizes and contents. The mixed powder was laser sintered at various input energy levels. The results indicated that porosity increased as the NaCl particle size decreased, and this effect became more significant with higher NaCl content.

Introduction

Porous materials possess unique properties such as low weight, permeability, sound absorption, and biocompatibility, attributes not typically found in dense materials. These characteristics make them attractive for a wide range of applications, including aerospace structural components, catalyst supports, filtration membranes, and biomedical scaffolds. The performance of these materials is highly dependent on their internal pore structures, including porosity, pore shape, and interconnectivity. Therefore, control of pore architecture is essential for achieving the desired functionality [1].

Recently, additive manufacturing (AM) technologies have garnered attention as a means of designing and controlling pore structures. Among these, lattice structures, which enable control of porosity through design, have been extensively studied for their potential in applications requiring lightweight structures, energy absorption, and enhanced biocompatibility [2–5]. Polymer-based powder bed fusion using a laser beam (PBF-LB/P) is particularly suitable for complex geometries, as it does not require support structures. This advantage has resulted in its increased adoption in the design of multifunctional structures. However, lattice structures often result in relatively large pore sizes owing to limitations in printing resolution, which can reduce the specific surface area. Although PBF-LB/P parts inherently contain micropores, it remains challenging to reproducibly fabricate highly porous and interconnected structures that significantly exceed the initial packing density of the powder [6].

To address this issue, a novel approach has been proposed where a soluble filler is mixed with the base powder and subsequently removed after fabrication to create pores [7–9]. For instance, Niino et al. demonstrated that mixing NaCl with polycaprolactone (PCL) and eluting it with water results in highly interconnected structures [7,8]. Yan et al. developed a high-permeability filter with hierarchical porosity by mixing a soluble filler with nylon powder [9]. These studies suggest that porosity can be controlled to some extent by adjusting the volume fraction of the filler. However, the actual porosity often deviates from the designed value owing to changes in powder flowability and sintering behavior caused by the filler [9-11]. In particular, when using high concentrations of fine inorganic fillers, both powder flowability during recoating and melt flowability during sintering tend to deteriorate, thereby increasing the risk of unsintered voids and interlayer defects [10,11]. Furthermore, the particle size and filler content can affect the interfacial behavior with the base polymer and interlayer bonding strength, ultimately influencing the final pore structure [12].

In this study, polyamide 12 (PA12) powder was mixed with NaCl particles of various sizes and processed using PBF-LB/P. The primary objective was to investigate the effect of the filler particle size on the resulting porosity. Additionally, the relationship between the powder characteristics, such as packing density, flowability, and porosity, was examined.

Materials and Methods

Materials

Polyamide 12 (PA12) powder (PA12smooth, Sinterit) was used as the base material. According to the technical datasheet, the particle size of PA12 Smooth ranges from approximately 19 to 90 μm , with a median diameter of about 38 μm . A 7:3 mixture of recycled and virgin PA12 powders was prepared for the experiments. Sodium chloride (NaCl) was used as soluble filler. After pulverization, the NaCl powder was classified into three particle size ranges—below 53 μm , 53~100 μm , and 100~150 μm —using standard sieves. These particle size ranges were selected based on practical considerations in the PBF-LB/P process. The upper limit (~150 μm) was determined to correspond to the commonly used layer thickness range (approximately 100–150 μm), and the powders were divided into three ranges accordingly. The particle size distributions of the NaCl powders are illustrated in Figure 1. Figure 2 presents magnified images comparing the morphologies of NaCl powders in each particle size range. Mixtures of PA12 and NaCl powders were used for fabrication, with NaCl contents set at 30, 40, and 50 vol%. Based on the true densities of PA12 (1.03 g/cm^3) and NaCl (2.16 g/cm^3), the corresponding mass ratios were calculated to achieve the desired volume fractions. Powder mixing was performed using a T2F mixer (WAB Co.) for more than one hour to ensure homogeneity.

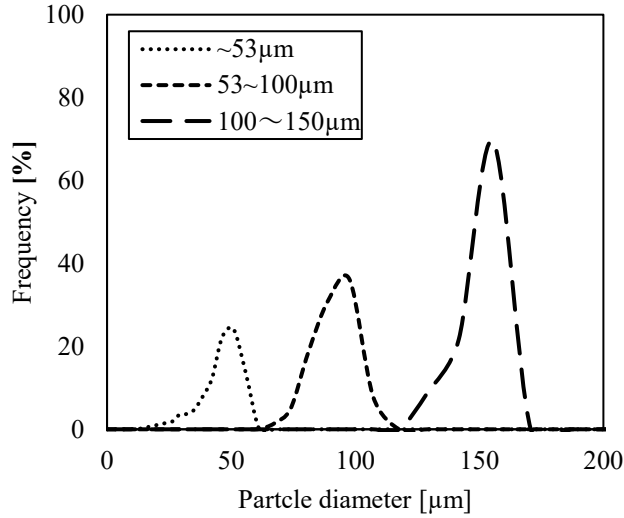


Figure 1. Particle size distribution of the NaCl powders. NaCl powders were classified into three particle size ranges and analyzed using a portable particle size analyzer (PITA, Seishin).

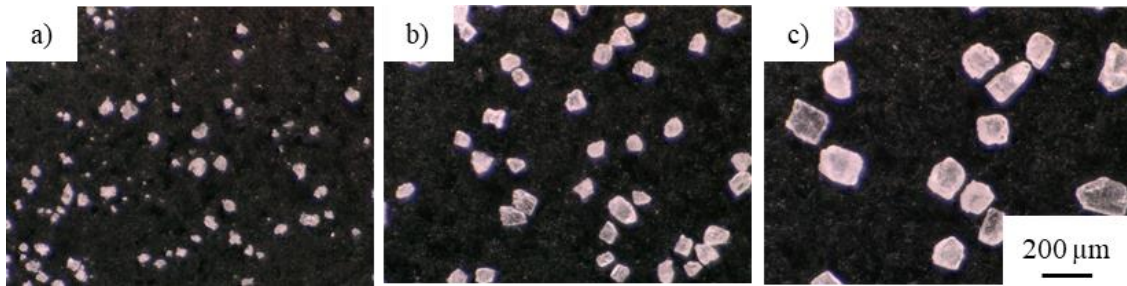


Figure 2. Morphology of NaCl powders in each particle size range: a) $\sim 53 \mu\text{m}$, b) $53\sim 100 \mu\text{m}$, c) $100\sim 150 \mu\text{m}$. All images were taken under the same magnification to allow direct comparison of particle shape and surface features.

Powder Characterization

The bulk density (ρ_{bulk}) and tapped density (ρ_{tap}) of the powder mixtures were measured to evaluate packing and flowability. Packing fraction ($\varphi_{packing}$) was calculated using Equation (1), and the Hausner ratio (HR) was calculated using Equation (2). The Hausner ratio (HR) is defined as the ratio of tapped density to bulk density. It is widely used as an indicator of powder flowability. The true density of the mixed powder ($\rho_{mix,true}$) was determined using Equation (3), based on the volume fraction of NaCl (MR_{NaCl}). Each condition was evaluated twice.

$$\varphi_{packing} = \frac{\rho_{bulk}}{\rho_{true}} \quad (1)$$

$$HR = \frac{\rho_{tap}}{\rho_{bulk}} \quad (2)$$

$$\rho_{mix,true} = \rho_{NaCl} \cdot MR_{NaCl} + \rho_{PA}(1 - MR_{NaCl}) \quad (3)$$

Fabrication Process of Porous Parts

An overview of the fabrication process for the porous parts is presented in Figure 3. A LisaPro system (Sinterit Co.) equipped with an infrared laser (wavelength: 808 nm) was employed for laser sintering. The fabrication parameters were configured using the dedicated Sinterit Studio Advanced software. The powder bed temperature was set to 175 °C, the layer thickness to 125 μm, and the hatch spacing (d_{hatch}) to 0.36 mm. The laser scanning speed (v) and power (P) could not be directly specified and were instead adjusted via a proprietary parameter called “energy scale.” In this study, the energy density (E), as defined by Equation (4), was controlled by varying the energy scale. Based on reference [13], the energy density of the LisaPro system was calculated and set at five levels ranging from 5.3 to 26.3 kJ/m². The model used for fabrication measured 10 mm × 10 mm × 5 mm, and five samples were produced for each condition.

After fabrication, the embedded NaCl was removed via dissolution with water. The samples were first held under vacuum (-0.1 MPa) for 3 hours to promote water penetration into the interior, followed by immersion under atmospheric pressure for 3 days to complete the dissolution process. The eluted samples were then left at room temperature (approx. 25°C) for more than one day and subsequently dried in an oven at 50 °C for 24 hours to obtain the final porous parts.

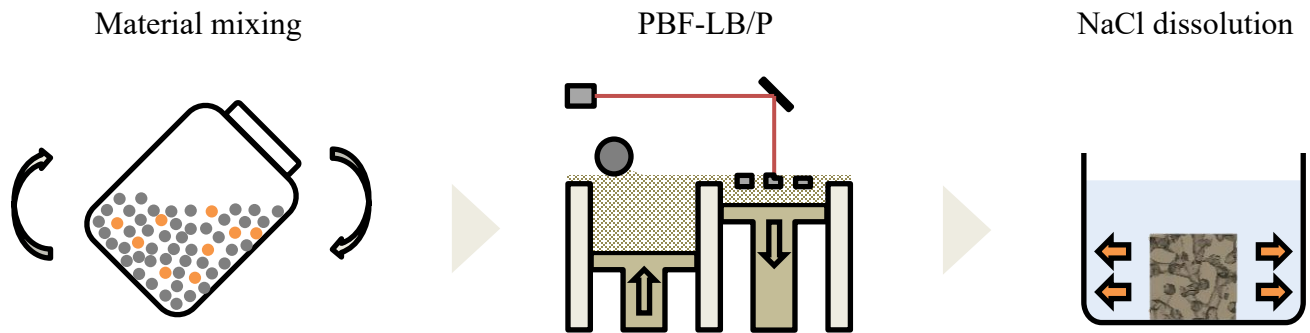


Figure 3. Fabrication process of porous parts. The process consists of powder mixing, laser sintering using the LisaPro system, and NaCl removal via vacuum-assisted water immersion.

$$E = \frac{P}{v \cdot d_{hatch}} \quad (4)$$

Confirmation of NaCl Dissolution via X-ray CT

To verify the dissolution of NaCl, the internal structure of the porous parts after dissolution was observed using an X-ray CT system (TOSCANER-30000 μ CM, Toshiba IT Control Systems). The scanning conditions were set to a tube voltage of 100 kV, a tube current of 50 μ A, and a voxel size of 18 μ m.

Porosity Measurement

The porosity (φ) of the fabricated porous samples was measured. Porosity was calculated using Equation (5), based on the measured density (ρ_P) of the samples. Density measurements were performed using the Archimedes method. To prevent water infiltration into the pores, a water-repellent spray was applied to the samples. Five samples were measured for each condition.

$$\varphi = \left(1 - \frac{\rho_P}{\rho_{PA}}\right) \quad (5)$$

Results and Discussion

Packing and Flowability of Mixed Powders

Figure 4 shows the relationship between the packing fraction and the mixture of PA12 and NaCl powders. As expected, the packing fraction decreased with decreasing NaCl particle size. For the finest particles (~ 53 μ m), the packing fraction decreased monotonically with increasing NaCl content. In contrast, for the coarsest particles (100–150 μ m), the packing fraction increased with higher filler content. For the intermediate particle size range (53–100 μ m), the packing fraction increased up to 30 vol% and then decreased as the NaCl content continued to rise.

Figure 5 presents the relationship between the mixing conditions and the Hausner ratio. In PBF-LB/P, powder flowability is considered good when the Hausner ratio is below 1.25, moderate between 1.25 and 1.4, and poor above 1.4 [14]. Flowability decreased with decreasing particle size. For powders with particle sizes below 53 μ m, the Hausner ratio exceeded 1.45, indicating significantly poor flowability. Conversely, NaCl powders with particle sizes of 100–150 μ m exhibited Hausner ratios below 1.25 across all mixing ratios, indicating excellent flowability.

These differences in behavior depending on the particle size can be attributed to particle agglomeration [14]. As the particle size decreases, intermolecular and electrostatic forces become more dominant than gravitational forces, leading to stronger cohesion. This increased agglomeration likely caused observed reductions in packing fraction and flowability of the mixed powder. Although smaller particles are typically used to obtain finer pores, agglomeration may result in the formation of large pores. Therefore, countermeasures to prevent agglomeration may be necessary. These results demonstrate that packing density varies with particle size. Because the pore size is currently controlled primarily by filler particle size, a thorough understanding of this relationship is essential. The influence of particle size on packing density and its subsequent effect on porosity is discussed in a later section. Notably, the bulk density (ρ_{bulk}) measured in this study closely approximates the powder bed packing density during PBF-LB/P fabrication [14,15].

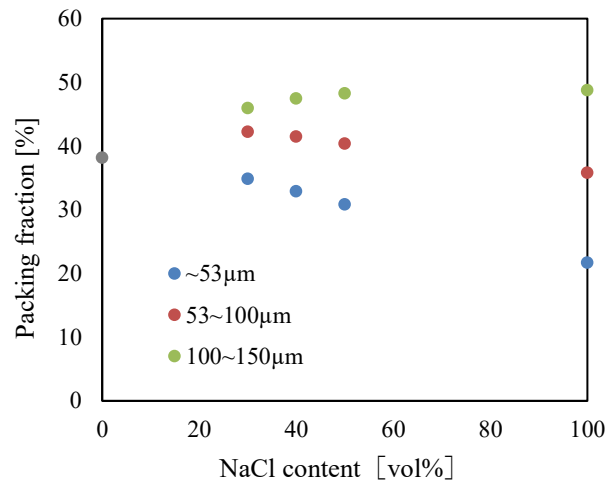


Figure 4. Packing fractions of powder blends. Packing fraction of PA12–NaCl powders as a function of NaCl size and content. Finer particles exhibited lower packing density. The graph plots the average values. Since the difference between the maximum and minimum measured values under each mixing condition was less than 0.1%, error bars were omitted

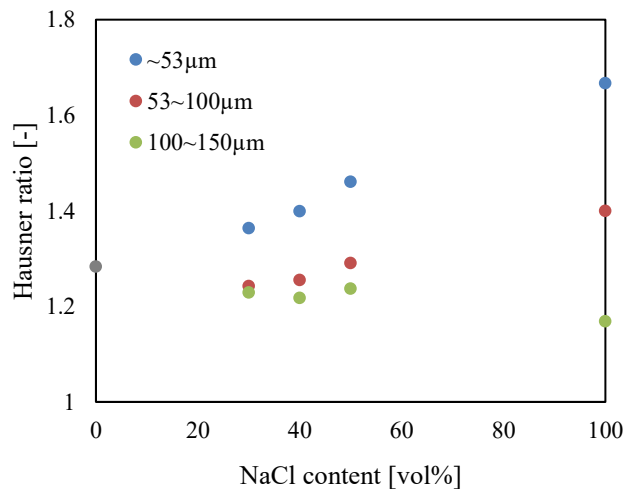


Figure 5. Hausner ratio of powder blends. Hausner ratios for different NaCl sizes and mixing ratios. Flowability decreased with finer NaCl powders. The graph plots the average values.

Confirmation of NaCl Dissolution via X-ray CT

Figure 6 depicts X-ray CT cross-sectional images of the sample a) before NaCl dissolution and b) after dissolution. These samples were fabricated under conditions of 30 vol% NaCl content and particle size below 53 µm.

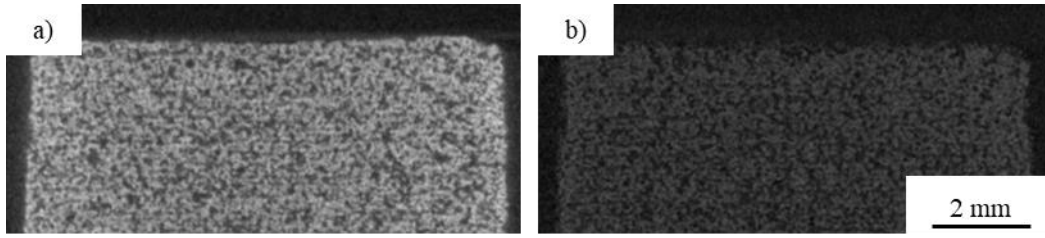


Figure 6. CT images a) before and b) after NaCl dissolution. Cross-sectional CT images of samples fabricated with 30 vol% NaCl and particle size below 53 μm , before and after dissolution. Bright regions represent NaCl; dark regions indicate pores. The images are from different samples.

Figure 7 presents post-dissolution observations for samples with the lowest NaCl content (30 vol. %), a condition under which incomplete dissolution was initially anticipated. The observations focused on variations in NaCl particle size and laser energy density. Among the tested five energy density levels, three representative values—minimum (5.3 kJ/m^2), intermediate (15.8 kJ/m^2), and maximum (26.3 kJ/m^2)—are shown. No high-brightness particle-like features were observed in any of the samples, indicating that NaCl was completely eluted in all cases. In Figure 9, the lower portion of the image, affected by the sample holder, was removed for clarity. Notably, the linear dark regions observed under low energy density conditions are attributed to insufficient melt bonding between PA12 layers. Based on these X-ray CT observations, the porosity values obtained using the Archimedes method, described in the following section, were considered reliable and unaffected by residual NaCl.

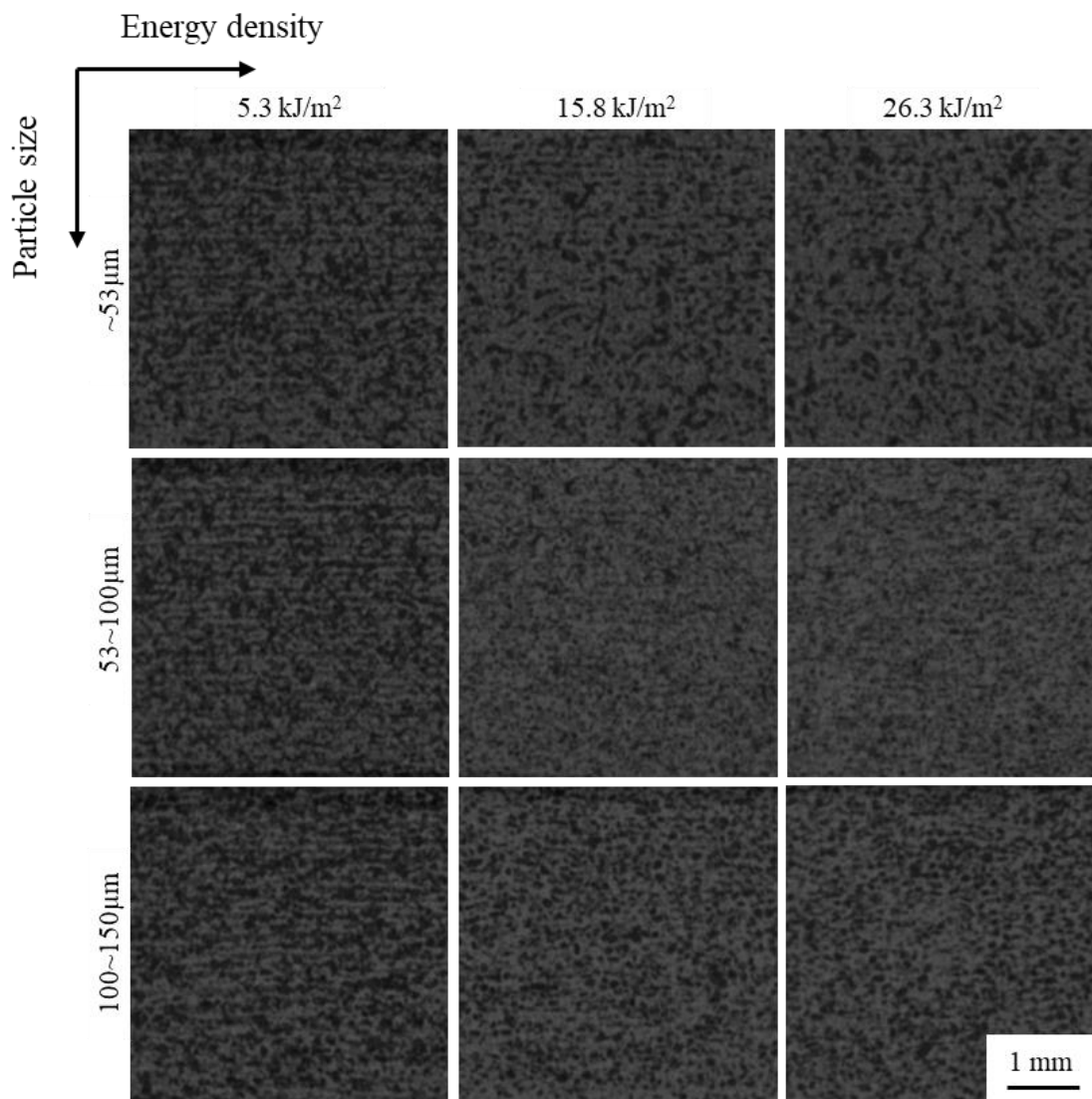


Figure 7. Confirmation of NaCl removal. Complete dissolution of NaCl was confirmed for all 30 vol% samples regardless of particle size or energy density. No residual filler was observed.

Effect of Soluble Filler Mixing Conditions on Porosity

Figures 8 illustrate the relationship between laser energy density and porosity for each NaCl mixing ratio. In all cases, porosity decreased with increasing energy density and tended to plateau beyond a certain threshold. This behavior was attributed to enhanced melting and flow of the PA12 resin throughout the powder bed, which filled the microvoids caused by unmelted particles. However, once the energy density reached a level where powder flowability became the limiting factor—referred to as the “flowability limit”—further increases in energy did not reduce porosity. At a constant mixing ratio, smaller NaCl particles resulted in higher porosity due to the increased specific surface area and interfacial area between PA12 and NaCl, which led to greater interfacial resistance during the melt flow process. In polymer systems containing inorganic fillers, it is well established that melt viscosity increases with higher filler content, smaller particle size, and greater

surface area [16]. This trend was also observed in this study. Specifically, under the condition of 50 vol% NaCl with particle sizes below 53 μm , flowability was severely restricted, and porosity remained nearly unchanged despite variations in energy density. Although the melt rheology measurements of mixed powders are ideal for quantitatively evaluating the flowability limit, such measurements were not conducted in this study because of the risk of NaCl corroding metal components of the equipment. Nevertheless, the observed dependence of porosity on particle size and mixing ratio is consistent with known viscosity-increasing mechanisms in filler-rich polymer systems, suggesting that both powder flowability and melt flow behavior are critical in determining final porosity.

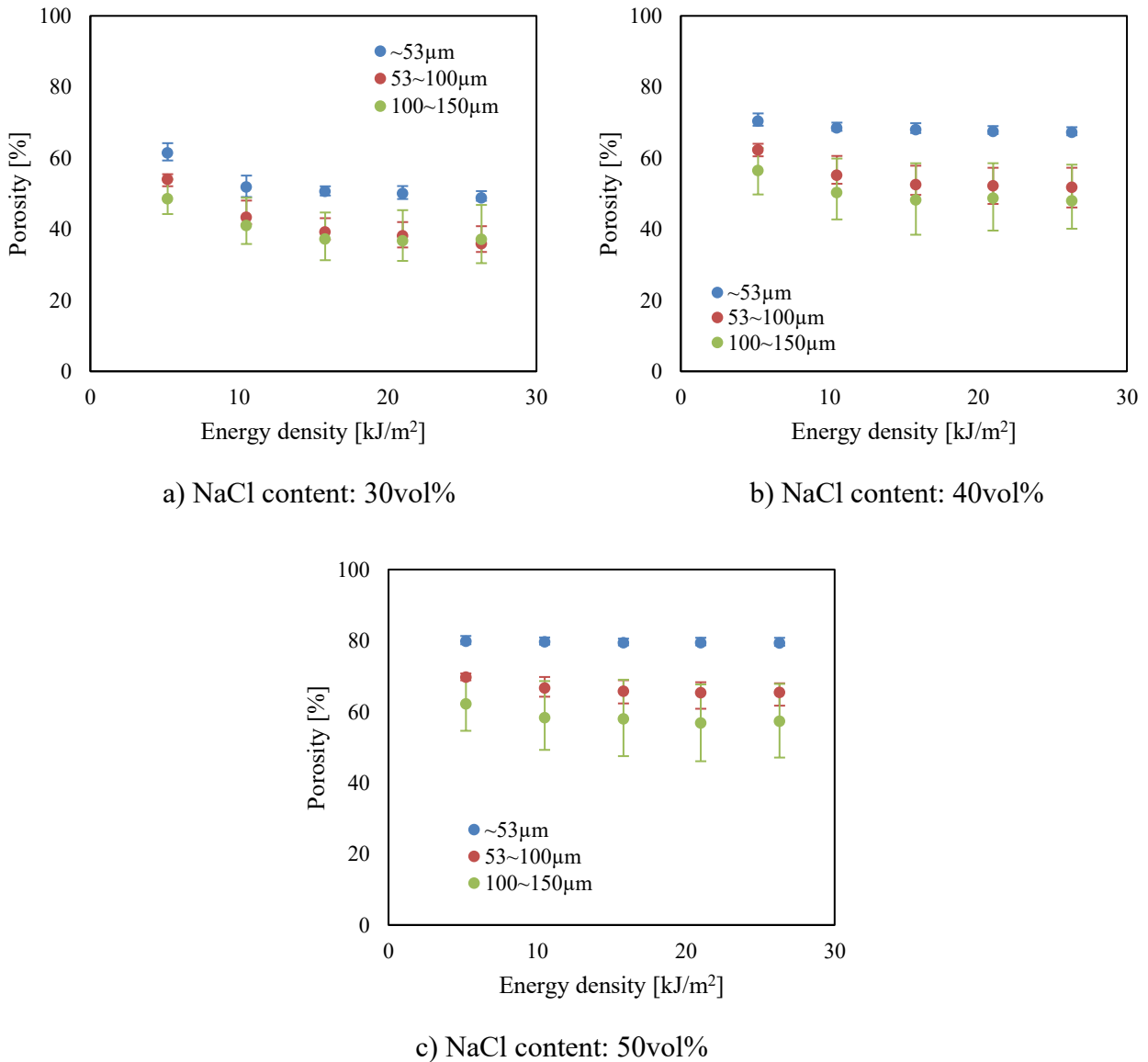


Figure 8. Porosity as a function of laser energy density for NaCl contents of a) 30 vol%, b) 40 vol%, and c) 50 vol%. Finer NaCl particles led to higher porosity because of reduced melt flow. Error bars indicate maximum and minimum values.

Figure 9 shows the measured porosity alongside two theoretical values corresponding to the volume fraction of NaCl under different mixing conditions. The first theoretical value represents the lower limit, assuming that the porosity equals the filler volume fraction. This corresponds to a case where PA12 is fully melted and fills all the gaps around the NaCl particles. The second theoretical value is the upper limit, calculated using the bulk and true densities of the powder blend. It assumes an idealized state in which PA12 does not flow at all, and the mixed powder solidifies in its initial packed state. All measured values lie between these two theoretical limits, indicating that flowability and sintering behavior of PA12 affect the pore structure. Particularly, under the fine particle condition ($\sim 53 \mu\text{m}$), the measured porosity approaches the theoretical upper limit, suggesting that molten PA12 did not sufficiently flow between NaCl particles, leaving the original powder void structure intact. Conversely, under the coarse particle condition ($100\sim 150 \mu\text{m}$), the measured values are close to the lower limit, implying that PA12 flowed well and filled the gaps between NaCl particles. Under fine-particle conditions, the porosity tended to approach the theoretical upper limit, making it easier to control. However, fine powders tend to aggregate, potentially causing issues with powder bed formation and pore size control. These results reveal that porosity is not determined solely by the filler ratio but is also influenced by factors such as particle size, powder packing density, and flow behavior during sintering.

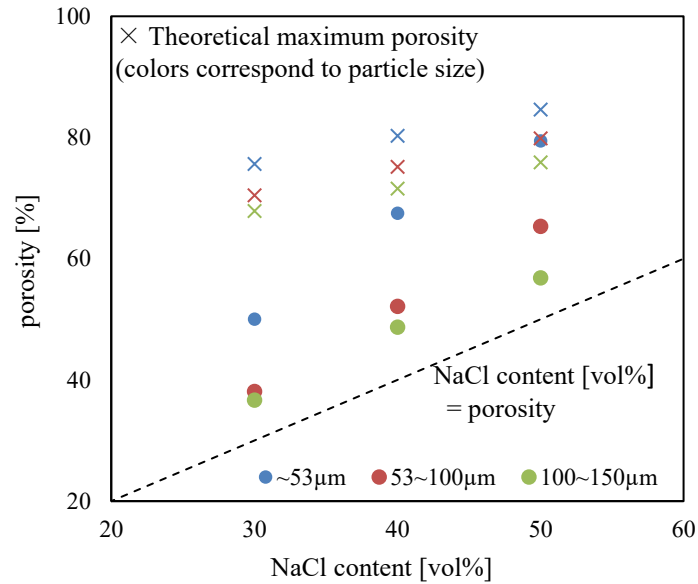


Figure 9. Comparison of measured and theoretical porosity. Porosity was compared with theoretical upper and lower bounds based on particle size and powder packing. Results indicate that both packing and melt behavior influence the final pore structure. Error bars are omitted for clarity.

Conclusion

In this study, the porous parts were fabricated using PBF-LB/P with NaCl as a soluble filler. The effects of NaCl particle size and mixing ratio on powder packing, flowability, and resulting

porosity were investigated. As particle size decreased, both packing density and flowability decreased, leading to reduced melt flow and increased porosity. Under fine particle conditions (~53 μm), particle aggregation lowered powder bed density, and porosity saturated regardless of energy input. In contrast, coarse particles exhibited better flowability and allowed for more stable porosity control. The measured porosity values lie between the theoretical lower and upper limits, indicating both powder packing and melt behavior influence the final pore structure. These results demonstrate that porosity is not solely governed by the filler content, but also by filler particle size. These findings provide a foundation for optimizing pore structures through appropriate filler selection and process control in future porous part designs.

Acknowledgment

This work was supported by JSPS KAKENHI Grant Number 23K03615. We would like to thank Editage (www.editage.jp) for English language editing.

Reference

- [1] L. J. Gibson and M. F. Ashby, *Cellular Solids: Structure and Properties*-Second edition, Cambridge, U.K.: Cambridge Univ. Press, 1997.
- [2] S. Okubo, Y. Yamauchi, and K. Kitazono, "Effects of random and controlled irregularity in strut lattice structure of PA12 on compression anisotropy," *Addit. Manuf.*, vol. 63, p. 103385, 2023.
- [3] P. Zhang et al., "Design and optimization of high stiffness tetrahedral lattice structure," *Addit. Manuf.*, vol. 102, p. 104719, 2025.
- [4] T. G. Zieliński et al., "Reproducibility of sound-absorbing periodic porous materials using additive manufacturing technologies: Round robin study," *Addit. Manuf.*, vol. 36, p. 101564, 2020.
- [5] N. Sabahi, I. Roohani, C. H. Wang, and X. Li, "Material extrusion 3D printing of bioactive smart scaffolds for bone tissue engineering," *Addit. Manuf.*, vol. 98, p. 104636, 2025.
- [6] C. Morano and L. Pagnotta, "Additive manufactured parts produced by selective laser sintering technology: Porosity formation mechanisms," *J. Polym. Eng.*, vol. 43, no. 6, pp. 537–555, 2023.
- [7] T. Niino, Y. Sakai, H. Hun, and H. Naruke, "SLS fabrication of highly porous model including fine flow channel network aiming at regeneration of highly metabolic organs," in *Proc. Solid Freeform Fabrication Symp.*, 2006, pp. 160–170.
- [8] T. Niino, S. Oizumi, and H. Otsuki, "Laser sintering fabrication of highly porous models utilizing water leachable filler: Experimental investigation into process parameters," in *Proc. Solid Freeform Fabrication Symp.*, 2007, pp. 494–502.
- [9] M. Yan, X. Tian, G. Peng, Y. Cao, and D. Li, "Hierarchically porous materials prepared by selective laser sintering," *Mater. Des.*, vol. 135, pp. 62–68, 2017.
- [10] Y. Zhang, L. Hao, M. M. Savalani, R. A. Harris, and K. E. Tanner, "Characterization and dynamic mechanical analysis of selective laser sintered hydroxyapatite-filled polymeric composites," *J. Biomed. Mater. Res. A*, vol. 86A, pp. 607–616, 2008.

- [11] S. Arai, S. Tsunoda, A. Yamaguchi, and T. Ougizawa, “Effects of short-glass-fiber content on material and part properties of poly(butylene terephthalate) processed by selective laser sintering,” *Addit. Manuf.*, vol. 21, pp. 683–693, 2018.
- [12] M. A. Spurek et al., “Influence of the particle size distribution of monomodal 316L powder on its flowability and processability in powder bed fusion,” *Addit. Manuf.*, vol. 95, p. 104512, 2024.
- [13] A. Sommereyns et al., “Light matters: Quantifiable optical interaction between near-infrared laser radiation and nano-additivated polymers in all states of matter present in laser powder bed fusion,” *Addit. Manuf.*, vol. 86, p. 104211, 2024.
- [14] I. Baesso et al., “Characterization of powder flow behavior for additive manufacturing,” *Addit. Manuf.*, vol. 47, p. 102250, 2021.
- [15] K. Wudy, L. Lanzl, and D. Drummer, “Selective laser sintering of filled polymer system: Bulk properties and laser beam material interaction,” *Phys. Procedia*, vol. 83, pp. 991–1002, 2016.
- [16] N. J. Mills, “The rheology of filled polymers,” *J. Appl. Polym. Sci.*, vol. 15, pp. 2791–2805, 1971.